Journal of Catalysis 277 (2011) 14–26

Contents lists available at ScienceDirect

Journal of Catalysis

journal homepage: www.elsevier.com/locate/jcat

Structure and catalytic performance of Pt-promoted alumina-supported cobalt catalysts under realistic conditions of Fischer–Tropsch synthesis

Héline Karaca [a], Olga V. Safonova [b,*], Stéphane Chambrey [a], Pascal Fongarland [a], Pascal Roussel [a], Anne Griboval-Constant [a], Maxime Lacroix [c], Andrei Y. Khodakov [a,*]

[a] UCCS, USTL-ENSCL-EC Lille, 59655 VIlleneuve d'Ascq, France
[b] Swiss-Norwegian Beamlines, ESRF, BP 220, 38043 Grenoble Cedex, France
[c] Total Petrochemicals Research Feluy SA, Refining and Marketing, Zone Industrielle C, 7181 Feluy, Belgium

ARTICLE INFO

Article history:
Received 16 May 2010
Revised 20 September 2010
Accepted 12 October 2010
Available online 24 November 2010

Keywords:
Fischer–Tropsch
Deactivation
Syngas
In situ
Operando
Time-resolved XRD

ABSTRACT

The structure of alumina-supported cobalt catalysts promoted with platinum and their catalytic performance in Fischer–Tropsch synthesis were investigated under realistic reaction conditions (P = 20 bar, T = 493 K) using *in situ* time-resolved X-ray diffraction with simultaneous analysis of reaction products. The catalysts were prepared via incipient wetness impregnation and characterized by a wide range of *ex situ* techniques. Direct *in situ* measurements were indicative of considerable versatility of alumina-supported cobalt catalysts during Fischer–Tropsch synthesis. Cobalt sintering occurred at the first hours of the reaction and resulted in a significant drop of the catalytic activity. In addition to sintering, partially oxidized catalysts containing smaller cobalt particles (mean particle size <5 nm) were slowly reducing during Fischer–Tropsch reaction. Treatment of cobalt catalysts in pure carbon monoxide led to selective transformation of cobalt metallic phases to Co_2C cobalt carbide. Cobalt carbidization followed by hydrogenation selectively led to cobalt *hcp* metallic phase, which seems to be more active in Fischer–Tropsch synthesis than cobalt *fcc* phase. Cobalt oxidation by water was not significant in the catalysts with metal particles larger than 5 nm even at high water concentrations.

1. Introduction

Low temperature Fischer–Tropsch synthesis produces clean hydrocarbon fuels and chemicals from syngas, which can be generated from natural gas, coal or biomass [1,2]. The process involves cobalt catalysts supported by refractory oxides (alumina, silica, titania, etc.). Since last two decades, cobalt catalysts have been used commercially by Sasol in South Africa and Qatar and Shell in Malaysia in both fixed bed and slurry bubble column reactors. It is usually considered that FT synthesis proceeds on cobalt sites, which are situated on the surface cobalt metal nanoparticles of 6–30 nm. For cobalt nanoparticles larger than 6–8 nm, it has been shown that FT turnover frequency (reaction rate normalized by the number of cobalt surface atoms) is invariant of the particle size, while for smaller cobalt particles (d < 6 nm) FT turnover frequency drops with a decrease in particle size [3]. The catalytic performance of cobalt FT catalysts can be enhanced by promotion with noble metals [2,4]. Besides the modification of the catalytic performance, noble metal promoters produce a variety of effects on the structure of cobalt FT catalysts: cobalt reducibility and/or cobalt dispersion, formation of bimetallic particles, formation of barely reducible cobalt support mixed compounds, decomposition of cobalt precursors, hydrogen activation... [4].

Catalyst deactivation is a major problem and has many challenges regarding FT synthesis [5]. It results in a loss in hydrocarbon productivity and requires repetitive catalyst regeneration or replacement. It has been largely shown that the rate of catalyst deactivation in FT synthesis depends on the catalyst, catalytic reactor and operating conditions (gas purity, flow rate, total pressure, H_2/CO ratio, temperature, carbon monoxide conversion). The deactivation behavior can also be affected by the catalyst structure: cobalt particle size, support chemistry and morphology. Promoters such as noble metals or oxides also change the reducibility and stability of cobalt phases under the reaction conditions [4–6].

Some of immediate and drastic consequences of catalyst deactivation can be avoided provided the mechanism of catalyst deactivation has been uncovered, and catalyst structure, reactor configuration and operating conditions have been optimized consequently [7]. The efficient control of catalyst deactivation under industrially relevant conditions is therefore crucial to attain high and long-lasting hydrocarbon productivity and to improve the overall economical efficiency of FT technology.

* Corresponding authors. Fax: +33 3 20 43 65 61.
E-mail addresses: olga.safonova@esrf.fr (O.V. Safonova), andrei.khodakov@univ-lille1.fr (A.Y. Khodakov).

0021-9517/$ - see front matter © 2010 Elsevier Inc. All rights reserved.
doi:10.1016/j.jcat.2010.10.007

It is clear that deactivation of cobalt FT catalysts is a complex phenomenon. Several mechanisms have been postulated previously to explain the deactivation behavior of supported cobalt catalysts: catalyst poisoning with sulfur or nitrogen containing compounds, cobalt oxidation, carbon deposition, carbidization, cobalt sintering, cobalt loss/leaching during the reaction, surface reconstruction, catalyst attrition... Most probably, the deactivation of cobalt FT catalysts is interplay of several phenomena. The deactivation can occur over different time scales: seconds, hours, days or months. In addition, catalyst deactivation can be reversible or irreversible and it can affect to a different extent the catalytic performance of cobalt catalysts. The paragraphs below focus on the catalyst deactivation mechanisms relevant to cobalt sintering, cobalt carbidization and cobalt oxidation. Others phenomena, which might be responsible for the deactivation of cobalt catalysts in FT synthesis, have been recently reviewed by Tsakoumis et al. [8] and Saib et al. [9].

1.1. Cobalt sintering

Cobalt crystal growth or cobalt sintering during the reaction has been suggested by several authors [10,11] as a possible cause of FT catalyst deactivation. Two conceptual models for crystallite growth due to sintering have been proposed: (A) atomic migration (or Ostwald ripening) or (B) particle migration (or particle migration and coalescence). Particle migration involves the migration of entire particles over the support followed by collision and coalescence. Atomic migration or ripening involves detachment of metal atoms from crystallites, migration of these atoms over the support surface and ultimately their capture by larger crystallites. The reacting atmosphere can affect the mechanism of sintering. A reaction of cobalt with carbon monoxide for example can generate volatile carbonyls, which would facilitate metal sintering. In general, sintering is an irreversible process. Very rarely sintering results in zero surface area of metal phase, more commonly sintering is limited by a non-zero dispersion observed after longer sintering times.

Overett et al. using *ex situ* characterization have shown [12,13] that cobalt sintering under FT conditions occurs rapidly during the first few days of use and tapers off after 10–20 days. The Co crystallite size increased rapidly over the first 10 days of FTS from 10 nm to 14–16 nm, after which the crystallite size appeared to stabilize. Overall, sintering could be responsible for roughly 25–40% of the long-term loss of catalyst activity. Very slight cobalt sintering in $CoRu/Al_2O_3$ in fixed bed reactor was observed by Tavasoli et al. [14]. A significant increase in cobalt particles sizes after high CO conversion run under 3.5 MPa pressure was observed by TEM in $Co–Re/SiO_2$ catalysts [15]. On the basis of EXAFS data, cobalt sintering was suggested as a major cause of deactivation of alumina-supported cobalt catalysts [16,17]. It was assumed [18] that water produced during FT synthesis increased the oxidation–reduction cycles on the catalyst surface and therefore enhances sintering rate of supported metals. Recently, Bezemer et al. [19] observed cobalt sintering in the presence of H_2/H_2O mixtures on cobalt catalysts supported by carbon nanofiber using *in situ* Mossbauer spectroscopy.

Sintering is usually considered as one of the causes of catalysts deactivation and leads to the loss of catalytic activity. It should be noted, however, that sintering could also have positive inference on the reaction rate if a stronger interaction of cobalt with a promoter can be enhanced in the catalysts. Jacobs et al. [20] found that the oxidation–reduction treatments of Ru-promoted Co/Al_2O_3 catalyst assisted in sintering of the metallic clusters to a larger size and promoted mixing on at least the order of the nanoscale. The larger crystallites in closer proximity to the Ru promoter led to a more facile cobalt reduction. In addition, a catalyst exposed to two oxidation–reduction cycles resulted in slightly higher conversion, higher α-value product, slightly lower methane selectivity, and greater stability than a reduced freshly calcined catalyst.

1.2. Carbidization

The hypothesis that FT synthesis proceeds via intermediate formation of a metal carbide was first suggested by Fischer and Tropsch [21]. A number of FT reaction mechanisms involve surface cobalt carbide which forms during the reaction as an intermediate. It has been shown [22–24] that bulk cobalt carbide is not active in FT synthesis. The catalysts converted to cobalt carbide in pure CO at 453 K did not show any noticeable activity. It was also shown that catalyst carbidization was reversible; the catalytic activity of carbided catalysts can be restored by subsequent treatment in hydrogen. In the used catalysts, which were exposed to syngas at atmospheric pressure for several hours, no cobalt carbide was detected by *ex situ* X-ray diffraction [22]. Cobalt catalysts typically contained cobalt *fcc* phase, while hydrogenation of cobalt carbide resulted in selective formation of cobalt *hcp* hexagonal phase.

It has been shown that bulk carbide can form during FT reaction under hydrogen lean conditions [25]. Ducreux et al. [26,27], however, have observed formation of cobalt carbide during FT synthesis even at a large excess of hydrogen. Under conditions favoring methanation ($H_2/CO = 9$ and $P = 3$ bar), formation of Co_2C phase was observed by *in situ* XRD on Co/Al_2O_3 and Co/TiO_2 catalysts after 70 h on stream, while on Co/SiO_2 the *in situ* XRD analysis did not reveal any particular structural transformation even after 310 h of the reaction. This also suggests that cobalt carbide formation is strongly affected by the support. The *in situ* experiments also showed a progressive decrease in carbon monoxide conversion on Co/Al_2O_3 and Co/TiO_2 catalysts, which coincides with an increase in the intensity of Co_2C XRD patterns. Under the same reaction conditions, neither carbide formation nor significant decrease in FT catalytic activity were observed on Co/SiO_2 catalysts.

1.3. Cobalt oxidation

Oxidation by water produced by FT reaction ($nCO + (2n + 1)H_2 = C_nH_{2n+2} + nH_2O$) has been considered for many years as a major cause of catalyst deactivation [9]. Although oxidation of bulk cobalt is not favorable, oxidation of nano-sized cobalt crystallites could be thermodynamically possible under the realistic conditions of FT synthesis [9,28]. This is due to significant contribution of the surface energy of nano-sized cobalt crystallites to the overall oxidation process. Assuming spherical morphology of nanoparticles, under realistic conditions of FT synthesis ($p_{H2O}/p_{H2} < 1.5$) metallic cobalt crystallites smaller than 4–5 nm were expected to be unstable and could be re-oxidized to CoO. After reconciliation of different literature data, Saib et al. [9] recently suggested that cobalt oxidation under realistic FTS conditions did not occur for metal crystallites larger than 2 nm. Several papers reported cobalt oxidation during FT reaction on the basis of *ex situ* characterization. Davis and co-workers [29–35] have performed XAS analysis of supported cobalt catalysts withdrawn from the liquid phase of the laboratory slurry reactor. Inside the reactor and during the analysis, the catalyst samples were suspended in FT wax. The authors believe that coating in wax prevents cobalt catalysts from oxidation. Analysis of XANES derivatives was indicative of partial re-oxidation of cobalt metal particles during FT synthesis.

It is often suggested, cobalt oxidation is caused by water. Thus, addition of water to FT feed should strongly affect the catalyst deactivation. Indeed, this is consistent with a few observations. It is known [36,37] that higher water partial pressures constantly lead to irreversible deactivation of FT catalysts. Apparently, the effect of smaller concentrations of water differs considerably depending on the catalyst support. According to Davis et al. [36]

for titania-supported catalyst, there is no effect of water addition on the catalytic performance. Silica-supported catalysts show even an improvement in FT reaction rate [38] when water is co-fed. Similar results were obtained by Krishnamoorthy et al. [39]. Alumina-supported catalysts usually lose their activity when water is added [36,37,40]. Botes [41] estimated that the reaction rate over the 25% Co/Al_2O_3 catalyst is not much affected by water up to a CO conversion of 60% when a dry syngas feed is applied. It seems, however, that oxidation by water could only involve surface and subsurface layers of cobalt metal particles. According to Sasol [42,43] researchers who conducted extensive *ex situ* studies of both used cobalt catalysts and *in situ* characterization with model H_2O/H_2 gas mixtures [43,44], cobalt bulk re-oxidation is not a significant deactivation mechanism of cobalt catalyst under commercially relevant FT conditions.

1.4. Why available data about deactivation of cobalt FT catalysts are so contradictory?

Thus, the literature exhibits a large divergence [8,42] concerning the mechanisms of deactivation of cobalt catalysts under the conditions of FT reaction. Two reasons could be responsible for this divergence.

First, different catalyst preparation, activation [42] and reaction procedures are often employed by different research groups. The catalyst can be prepared using a large variety of supports (alumina, silica, titania, carbon materials) and cobalt precursors (cobalt nitrate, cobalt acetate, cobalt organic complexes). The catalyst can be synthesized using different routes (incipient wetness impregnation, slurry impregnation, coprecipitation, deposition–precipitation, etc.) [2]. It can contain cobalt particles of different size. The catalyst activation procedure could involve cobalt calcination and reduction at different temperatures, different space velocities, different atmospheres [45]; the procedure of syngas introduction could also vary, which could result in a temperature hike in the reactor and thus, in catalyst deactivation. Catalyst deactivation mechanism could be a function of the operating conditions: syngas purity, syngas composition, reactor, pressure, temperature, carbon monoxide conversion, etc.

Second and most important, the divergences in the literature about the mechanism of deactivation of cobalt FT catalysts are likely to be related to *the lack of direct catalyst characterization techniques*. Indeed, the structure of working cobalt catalysts could be very sensitive to the reaction conditions and can be different from the structure of used counterparts. In particular, cobalt catalysts could be readily re-oxidized after their withdrawal from the catalytic reactor. In addition, it is also known that the surface of cobalt particles can undergo considerable restructuring under the conditions of FT reaction. Wilson [46,47] studied restructuring of Co(0 0 0 1) single crystal surface using STM. Significant alternations of cobalt surface were observed after 1 h of FT reaction (H_2/CO = 2, P = 4 bar, T = 523 K). The restructuring of cobalt single crystals under these conditions could result from exposure of the catalyst to carbon monoxide, water, high pressure and high temperature.

Thus, it appears that reliable information about the mechanism of catalyst deactivation could be only obtained by using *in situ* direct characterization techniques. *In situ* characterization of catalyst structure under realistic FT reaction conditions represents a significant experimental challenge because of high temperature, high pressure, presence of a large number of reaction products, multiphase reacting medium. Note that most of previous studies on the deactivation of cobalt FT catalysts have been limited either by *ex situ* characterization or by *in situ* measurements in the conditions, which are different from those typically used for FT synthesis (e.g. low syngas pressure [48], higher H_2/CO ratio favoring methanation [26,27], model "simulated" gas mixtures, etc.). Only recently, the *in situ* studies under industrially relevant conditions of FT synthesis have become possible [49,50]. *In situ* XRD seems to be particularly suitable for investigation into supported FT catalysts, which are constituted by supported cobalt particles of several nanometers and involve several elementary unit cells. Most importantly, XRD is one of very few techniques, which can provide information about catalyst structure *in situ* under realistic reaction conditions (e.g. P = 20 bar, H_2/CO = 2, T = 493 K) when the catalyst has become inaccessible to other characterization methods. The X-ray studies using synchrotron radiation source are well suited for *in situ* time-resolved measurements of the evolution of the catalyst containing small cobalt nanoparticles, as the high brilliance of the synchrotron source allows fast acquisition of X-ray scattering and diffraction patterns even for most demanding systems. Thus, the *in situ* XRD studies under FT realistic conditions are expected to provide more reliable information about the structure of working catalysts than *ex situ* investigation into spent catalysts.

The present work addresses structural modifications of supported cobalt catalysts studied at a wide range of realistic FT reaction conditions using *in situ* X-ray diffraction combined with online evaluation of catalyst performance. Alumina-supported cobalt catalysts promoted with small amounts of platinum and containing smaller and larger cobalt particles were characterized in this work at different stages of their preparation and activation by a large number of *ex situ* techniques.

2. Experimental

2.1. Catalyst preparation

Cobalt catalysts, containing 25 wt.% Co and 0.1 wt.% Pt (Table 1), were synthesized via two steps incipient wetness co-impregnation using aqueous solutions of cobalt nitrate ($Co(NO_3)_2\ 6H_2O$) or cobalt acetate ($Co(CH_3COO)_2\ 4H_2O$) and tetramine platinum nitrate ($Pt(NH_3)_4(NO_3)_2$). Commercial Puralox SCCA-5/170 alumina manufactured by Sasol with S_{BET} = 165 m^2/g, pore diameter of 8.3 nm and total pore volume of 0.477 cm^3/g was used as a catalytic support.

The impregnated solids were dried and calcined in air flow at 573 K or 773 K for 10 h (ramp 1 K/min, GHSV = 1000 $ml/g_{cat}/h$). After calcination, the samples were sieved to remove catalyst particles smaller than 50 μm. Cobalt and platinum contents in the catalysts were measured by X-ray fluorescence at the Analytical Service of Total Petrochemicals Research (Feluy, Belgium). The elementary analysis data are in good agreement with the theoretical values. The catalysts are labeled as **$CoPt/Al_2O_3$–P** where **P = N or A** designate, respectively, cobalt nitrate or acetate used for catalyst synthesis. $CoPt/Al_2O_3$–N1 and $CoPt/Al_2O_3$–A were calcined in air flow at 573 K, while $CoPt/Al_2O_3$–N2 was calcined at 773 K. Reference cobalt aluminate was obtained by calcination of $CoPt/Al_2O_3$–N catalyst at 1073 K for 5 h.

2.2. Ex situ catalyst characterization

The catalysts have been characterized at different preparation steps by a wide range of *ex situ* techniques. The BET surface area and pore size distribution were measured using nitrogen sorption at 77 K. Prior to the experiments, the samples were outgassed at 423 K for 5 h. The isotherms were measured using a Micromeritics ASAP 2010 system. The total pore volume (TPV) was calculated from the amount of vapor adsorbed at a relative pressure close to unity assuming that the pores are filled with the condensate in liquid state. The pore size distribution curves were calculated

Table 1
Alumina-supported cobalt catalysts.

Catalyst	Cobalt precursor	Cobalt content, wt.%	Platinum content, wt.%	S_{BET}, m^2/g	Total pore volume, cm^3/g	Diameter of cobalt oxide crystallites from XRD, nm
$CoPt/Al_2O_3$–N1	Nitrate	25	0.1	115	0.281	11.4
$CoPt/Al_2O_3$–N2	Nitrate	25	0.1	111	0.292	11.6
$CoPt/Al_2O_3$–A	Acetate	25	0.1	123	0.301	6.0

from the desorption branches of the isotherms using Barrett–Joyner–Halenda (BJH) formula [51]. (Table 1). The particle size distributions in the support and catalysts were measured using L230 Beckman-Coulter laser granulometer. The morphological and microchemical analyses were performed with a Philips SEM 505 scanning electron microscope equipped with an EDX Philips 505 microprobe at 5 and 20 keV. Transmission electron microscopy measurements were performed using JEOL 2000 FX//II equipped by STEM module and INCAx-Sight EDSX detector. The images were taken using CCD Olympus Keenview and Analysis iTEM software. Cobalt particle size in the calcined catalysts was measured directly from the TEM images. Prior to the measurements, the sample grains were coated under vacuum with acrylic resin. Then, they were cut using ultra-microtomy into slices of 150 nm thickness and deposited on a grid prior to the measurements.

The *ex situ* X-ray absorption spectra at Co absorption K-edge were measured at DUBBLE-CRG beam line, ESRF, France. The X-ray absorption measurements were performed in transmission mode; two ionization chambers were used for X-ray detection. The Si(1 1 1) double-crystal monochromator was calibrated by setting the first inflection point of K-edge spectrum of Co foil at 7709 eV. The X-ray absorption data were analyzed using the conventional procedure. The XANES spectra after background correction were normalized by the edge height. After subtracting the metal atomic absorption, the k^1-weighted EXAFS signal was transformed without phase correction from k space to r space. Crystalline Co_3O_4 and cobalt aluminate were used as reference compounds for XANES and EXAFS analysis.

The *ex situ* XRD patterns were recorded in the UCCS laboratory by a Siemens D5000 diffractometer using Cu Kα radiation and at BM01B-SNBL beam line, ESRF, France (λ = 0.5 Å, Si(1 1 1) channel cut monochromator) using the two-cycle diffractometer equipped by six detectors having Si(1 1 1) analyzer crystals and Na-I scintillation counters. The temperature-programmed reduction (TPR) was carried out in AutoChem II 2920 (Micromeritics) using 0.1 g of the sample in 5 vol.% H_2/Ar stream. The temperature ramping rate was 5 K/min.

2.3. Catalytic tests

The catalytic performance of alumina-supported cobalt catalysts was evaluated both in a conventional laboratory fixed bed stainless steel reactor (d = 13 mm) and in the capillary cell reactor [49,50] (which was also used for simultaneous *in situ* XRD measurements). Due to a significant volume and slow hydrodynamic response, the conventional fixed bed reactor was only used for the steady-state evaluation of catalytic performance. The catalyst loadings were 1 g in the conventional fixed bed reactor and 7–9 mg in the capillary cell. Prior to the catalytic tests, the catalysts were reduced in hydrogen for 10 h at 673 K in the conventional fixed bed reactor and for 2 h at 623 K in the capillary cell reactor. During the reduction, the temperature ramp was 3 K/min in both reactors, the hydrogen flow rate was 8400 $cm^3/g_{cat}/h$ in conventional fixed bed reactor and about 100,000 $cm^3/g_{cat}/h$ in capillary reactor. Carbon monoxide contained small amounts of nitrogen or argon (5 mol.%), which were used as internal standards. Analysis of H_2, CO, CO_2, and CH_4 was performed using CTR-1 or molecular sieve columns, while gaseous and liquid hydrocarbons were separated on Poraplot Q and SimDist columns.

2.4. In situ time-resolved XRD measurements combined with on-line evaluation of catalytic performance

The *in situ* time-resolved XRD data were measured at the BM01B-SNBL beamline (ESRF, France) using a high resolution diffractometer (described above), a gas manifold system and a capillary cell reactor. The known amount of catalyst was loaded in the quartz capillary (OD = 1 mm, wall thickness = 0.020 mm) and pressed from both sides with quartz wool. The capillary was attached to the stainless steel holder using high temperature epoxy glue. A Cyberstar gas blower was used to control the capillary reactor temperature. The total pressure in the reactor (up to 20 bar) was regulated by a back pressure controller. The gas lines before and after the reactor were heated up to 493 K using Horst heating tape to prevent condensation of liquid products. The liquid and solid products (water and heavy hydrocarbons) were collected downstream of the reactor in the stainless steel container at room temperature. Before the FT tests, the catalysts were reduced in hydrogen flow at 623 K at atmospheric pressure (temperature ramp of 3 K/min) and cooled down to 333 K in H_2 flow.

To avoid heat spots and reactor runaway, the FT start up procedure was adapted for conventional fixed bed and capillary reactors. After the reduction, the catalyst was cooled down to 333 K for both reactors and exposed to the syngas (H_2/CO = 2) at atmospheric pressure. Then, the reactors were pressurized up to 20 bar, and temperature of the catalyst was risen up to 473 K under syngas flow with temperature ramp of 3 K/min for the conventional fixed bed reactor and 3 K/min for capillary reactor. After dwelling at 473 K, the temperature was increased to 493 K with a ramp of 0.05 K/min for conventional fixed bed reactor and 1 K/min for capillary reactor. The time-resolved XRD patterns were recorded *in situ* under gas flows at desired temperatures and pressures. The measuring time per a XRD pattern in the 2θ range between 9.2° and 21.5° was close to 10 min. Simultaneous analysis of the reaction products was conducted using Agilent MicroGas-Chromatograph. The time of chromatographic analysis was about 7 min. Carbon monoxide conversion and methane selectivity were calculated from carbon monoxide, methane and argon or nitrogen chromatographic peaks. The XRD profiles were analyzed by FullProf program package using full profile matching [52]. To estimate the concentration of cobalt *fcc* and *hcp* phases in the working catalysis, quantitative Rietveld analysis was performed using constant isotropic Debye–Weller factor.

The mean crystallite particle size was calculated from XRD patterns using the Scherrer method. Scherrer [53] showed that, when a parallel monochromatic radiation falls on a random oriented mass of crystals, the diffracted beam is broadened when the crystallite size is small. By an approximation method, he obtained an expression for the integral breadth B of the diffracted beam in the following form: $B = K \cdot \lambda/(L \cdot \cos\theta)$ where λ is the wavelength of the incident X-rays, L is the crystallite size, θ is the Bragg angle

and K is a numerical constant for which the value of $2(\ln 2\pi)^{1/2} = 0.93$ was obtained. The standard reference material Silicon (Si), (NIST SRM 640c from the National Institute of Standards, NIST), was used to account for the diffractometer-alone broadening, taking care that all measurements were performed at the same wavelength and with the same primary and secondary optics. It thus allowed us to calculate the instrument resolution function, which was deconvoluted from the observed XRD patterns.

3. Results and discussion

3.1. Ex situ catalyst characterization

Representative SEM images of cobalt catalysts are shown in Fig. 1. They show polydispersed spherical particles with an average diameter of about 100 μm. SEM-EDX analysis suggests rather uniform cobalt repartition on the micrometric scale in cobalt catalysts prepared from cobalt nitrate or acetate. The particle size distribution curves (not shown) evaluated using laser granulometry indicate that both alumina support and supported cobalt catalysts are constituted by the grains with the average diameter of about 90 μm.

The XRD patterns of calcined cobalt catalysts prepared from cobalt nitrate and cobalt acetate (Fig. 2) exhibit peaks characteristic of γ-alumina and Co_3O_4. Calculation using the Scherrer equation and both 422 and 511 (λ = 1.54 Å and 0.5 Å) Co_3O_4 diffraction peaks [54,55] yields cobalt oxide average crystallite sizes about 10 nm in the catalysts prepared from cobalt nitrate and 6 nm in the catalysts prepared from cobalt acetate. In agreement with previous report [56], catalyst calcination at 773 K instead of 573 K does not produce any noticeable impact on the size of supported Co_3O_4 crystallites while using cobalt acetate as a precursor for catalyst synthesis significantly reduces cobalt particles size. Smaller cobalt oxide particles were previously detected in silica-supported catalysts [57–62], which were prepared from cobalt acetate. These results are also consistent with TEM images, which showed the presence of cobalt oxide particles of 5–15 nm in the calcined catalysts. In some cases, these individual cobalt oxide particles of 5–15 nm diameter agglomerate into aggregates of 100–200 nm. The size repartitions for cobalt oxide particles for $CoPt/Al_2O_3$–N1 and $CoPt/Al_2O_3$–A calculated from TEM images are shown in Fig. 3a and b. $CoPt/Al_2O_3$–N1 catalyst displays higher fraction of larger cobalt oxide particles than $CoPt/Al_2O_3$–A. Thus, both XRD and TEM data are indicative of smaller average cobalt particles size in $CoPt/Al_2O_3$–A than in $CoPt/Al_2O_3$–N1. Though both catalysts contain cobalt particles smaller than 5 nm, the concentration of these smaller particles is expected to be higher in $CoPt/Al_2O_3$–A than in $CoPt/Al_2O_3$–N1.

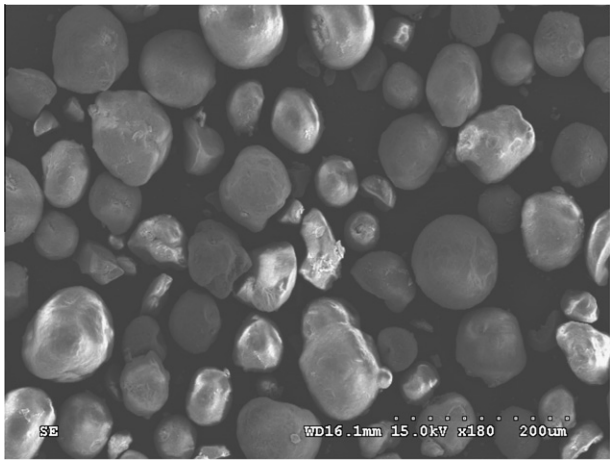

Fig. 1. SEM image of $CoPt/Al_2O_3$–N1 catalyst.

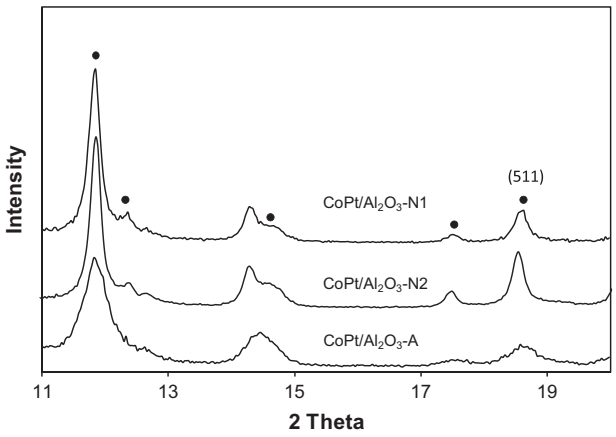

Fig. 2. XRD patterns of calcined cobalt catalysts (λ = 0.5 Å, ● indicates Co_3O_4 XRD peaks).

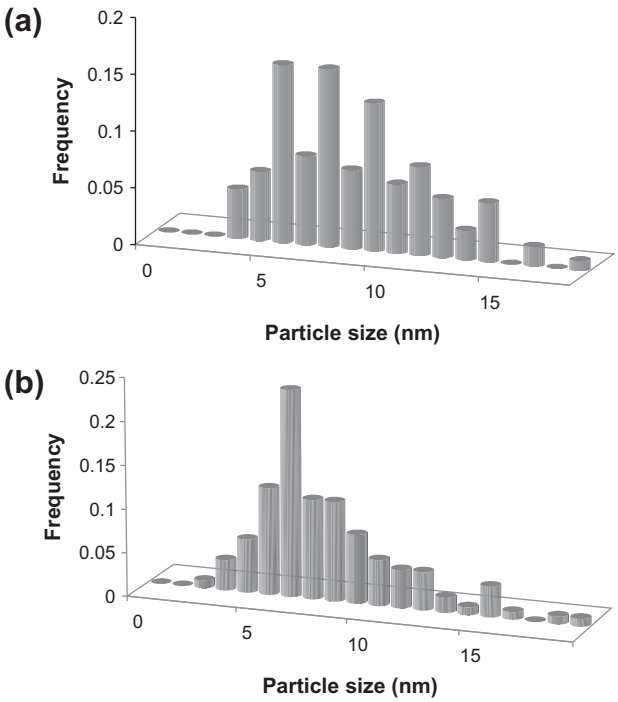

Fig. 3. Repartition of cobalt oxide particle sizes in calcined $CoPt/Al_2O_3$–N1 (a) and $CoPt/Al_2O_3$–A (b) catalysts from TEM data.

The XANES spectra and EXAFS Fourier transform moduli for calcined cobalt catalysts and reference Co_3O_4 and cobalt aluminate are shown in Fig. 4. The XANES spectra of calcined catalysts resemble the spectrum of bulk Co_3O_4. Two peaks at 1.34 and 2.3 Å and a shoulder at 2.9 Å are observed in the moduli of Fourier transform of EXAFS (Fig. 4b). In accordance with previous reports [63,64], the first peak at 1.34 Å is attributed to first CoO coordination shells for octahedral Co^{3+} and tetrahedral Co^{2+} sites. These two CoO coordination shells are usually not resolved in the Fourier transform moduli [63,64]. The peak and shoulder situated at 2.3 and 2.9 Å, respectively, were assigned to two CoCo coordination shells in Co_3O_4 [64]. Thus, Co_3O_4 seems to be a major phase in the calcined

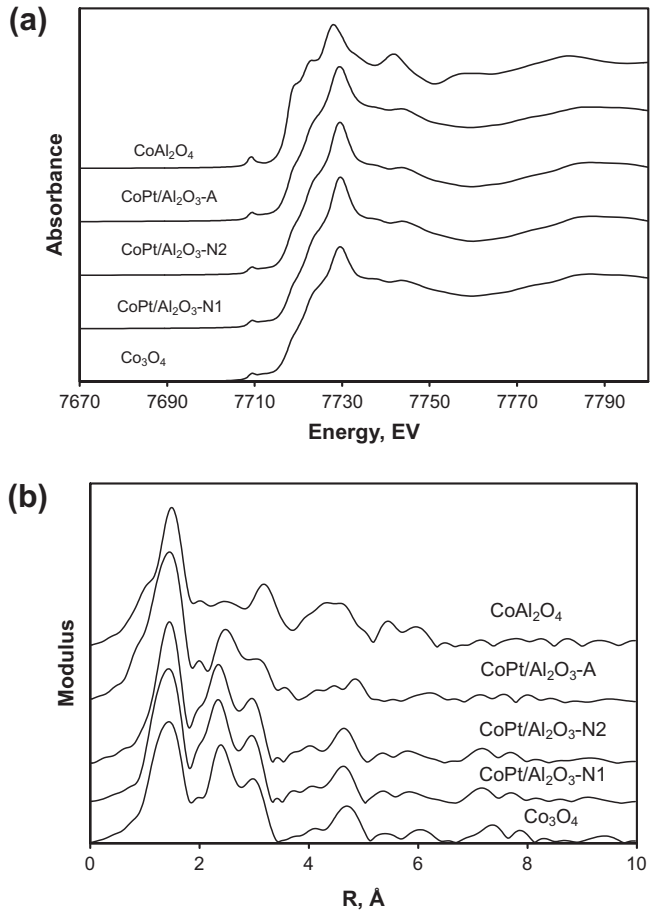

Fig. 4. XANES spectra (a) and EXAFS Fourier transform moduli (b) of calcined cobalt catalysts, reference Co_3O_4 and cobalt aluminate.

alumina-supported cobalt catalysts prepared from both cobalt nitrate and acetate. The XANES spectra were fitted using a linear combination of XANES spectra of reference Co_3O_4 and cobalt aluminate. This analysis showed that the fraction of Co_3O_4 phase was higher than 90% in all the studied calcined catalysts.

Fig. 5 shows the experimental TPR profiles of the calcined cobalt catalysts. They exhibit several hydrogen consumption peaks. Previous reports suggest [64–68] that the low temperature TPR peaks at 453–573 K could be attributed to partial reduction of Co_3O_4 to CoO, while the peaks observed at 573–823 K are assigned to the reduction of CoO to metallic cobalt. No TPR peaks above 923 K are observed for the catalysts prepared from cobalt nitrate and very low-intense peaks were observed for $CoPt/Al_2O_3$-A sample. This is indicative of a very low concentration of bulk barely reducible cobalt aluminate compounds in the catalysts. The TPR results are consistent with XANES and EXAFS data which also suggest low content of cobalt aluminates in the catalysts. Note that the low temperature TPR peaks of the $CoPt/Al_2O_3$–N1 catalyst exhibit doublets and shoulders at 490–500 K. The presence of doublets and shoulders can be due to the presence of residual NO_3^- species [69]. Indeed, in the present work nitrogen and nitrogen oxides were detected by mass spectrometry at the outlet of TPR apparatus at the temperature region corresponding to the doublet. Higher calcination temperature of the catalyst prepared from cobalt nitrate or use of cobalt acetate for catalyst preparation result in a slight shift of TPR profiles to higher temperatures. Note that our characterization and previous report [56] indicate that calcination temperature does not affect cobalt particle size in alumina-supported catalysts prepared from cobalt nitrate. Thus, in this case, the higher temperature shift of TPR peaks can be attributed to partial substitution of Co^{3+} in Co_3O_4 spinel framework by Al^{3+} ions from the alumina support [56,70]. Use of cobalt acetate for catalyst preparation leads to the formation of smaller cobalt oxide particles. It is known that smaller cobalt particles are much more difficult to reduce than larger ones [64]. Thus, a high temperature shift of TPR peaks in the case of the catalyst prepared from cobalt acetate probably also reflects a much more difficult reduction of smaller cobalt oxide particles rather than formation of barely reducible cobalt aluminate compounds.

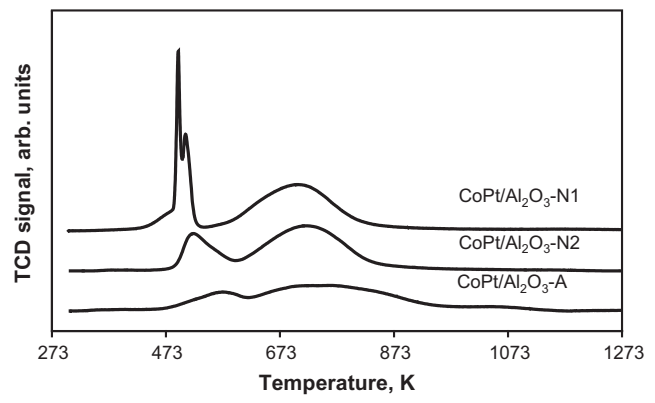

Fig. 5. TPR profiles of $CoPt/Al_2O_3$–N1 [50], $CoPt/Al_2O_3$–N2 [50] and $CoPt/Al_2O_3$–A catalysts (5%H_2/Ar, 5 K/min).

To summarize the results of *ex situ* characterization, the calcined cobalt catalysts prepared via impregnation of alumina with cobalt nitrate contain relatively larger cobalt oxide particles, while much smaller cobalt oxide particles are present in the catalyst prepared via impregnation with cobalt acetate. Larger cobalt oxide particles in $CoPt/Al_2O_3$–N1 and $CoPt/Al_2O_3$–N2 catalysts are much easier to reduce than smaller cobalt oxide particles in $CoPt/Al_2O_3$–A catalyst.

3.2. Steady-state catalytic tests in the conventional fixed bed reactor

The results of steady-state catalytic tests in the conventional fixed bed reactor at 20 bar, $H_2/CO = 2$ and 493 K are displayed in Table 2. The catalytic performance in FT reaction was typically measured after 3–5 days on stream. The FT reaction rates are expressed as cobalt-time yields; they were calculated from carbon monoxide conversion, inlet carbon monoxide partial pressure, gas–space velocity and amount of cobalt in the reactor. The accuracy in measuring FT reaction rates was about 5%.

The $CoPt/Al_2O_3$–N1 and $CoPt/Al_2O_3$–N2 exhibited much higher cobalt-time yields than $CoPt/Al_2O_3$–A. In agreement with the characterization data, the observed lower catalytic activity of the catalyst prepared from cobalt acetate could be attributed to lower reducibility of smaller cobalt particles and thus lower concentration of cobalt active sites. In addition, lower intrinsic FT turnover frequency on smaller cobalt particles could also contribute to lower activity of $CoPt/Al_2O_3$–A. This is also consistent with previous report by Bezemer et al. [3] who observed lower intrinsic activity of smaller cobalt particles in the catalysts supported on carbon nanofibers. In agreement with [3], higher methane selectivity was observed on smaller cobalt particles in $CoPt/Al_2O_3$–A.

After a catalytic test under standard conditions, $CoPt/Al_2O_3$–N1 catalyst was treated for 24 h with carbon monoxide at 493 K and $P = 20$ bar to convert cobalt into cobalt carbide. After the carbidization, the catalyst was again exposed to syngas ($H_2/CO = 2$) and showed zero activity in FT synthesis (Table 2). Then, the catalyst was treated with hydrogen for 24 h at 493 K. After purge with

Table 2
Catalytic performance[a] of alumina-supported cobalt catalysts in conventional fixed bed and XRD capillary cell reactors under quasi steady-state conditions (T = 493 K, P = 20 bar, H_2/CO = 2).

Catalyst	Reactor	GHSV, mol g^{-1} h^{-1}	X_{CO}, %	Cobalt-time yield, mol_{CO} s^{-1} mol_{cobal} t^{-1}	S_{CH4}, %	Productivity, g h^{-1} g_{cat}^{-1}	
						CH_4	C5+
$CoPt/Al_2O_3$–N1	Fixed bed	14,000	39.0	4.96×10^{-3}	8.0	0.09	0.70
Carbidized $CoPt/Al_2O_3$–N1	Fixed bed	14,000	0	0	–	–	–
Carbidized and hydrogenated $CoPt/Al_2O_3$–N1	Fixed bed	14,000	62.5	7.95×10^{-3}	8.6	0.17	1.03
$CoPt/Al_2O_3$–N1	Capillary	25,000	20.0	4.54×10^{-3}	5.0	0.06	–
Carbidized $CoPt/Al_2O_3$–N1	Capillary	25,000	0	0	–	–	–
Carbidized and hydrogenated $CoPt/Al_2O_3$–N1[b]	Capillary	25,000	33.0	7.50×10^{-3}	4.9	0.09	–
$CoPt/Al_2O_3$–N2	Fixed bed	10,500	41.0	3.91×10^{-3}	7.7	0.07	0.57
$CoPt/Al_2O_3$–N2	Fixed bed	14,000	30.0	3.81×10^{-3}	10.0	0.09	0.41
$CoPt/Al_2O_3$–A	Fixed bed	4900	28.2	1.25×10^{-3}	11.4	0.03	0.21
$CoPt/Al_2O_3$–A	Fixed bed	14,000	14.5	1.85×10^{-3}	7.2	0.03	0.14
$CoPt/Al_2O_3$–A[c]	Capillary	19,600	9.0	1.60×10^{-3}	8.6	0.03	–

[a] The accuracy in measuring cobalt-time yield was about 5%.
[b] Catalytic performance after 5 h on stream; steady-state was not attained.
[c] Catalytic performance after 8 h on stream; steady-state was not attained.

N_2, the regenerated catalyst showed a 50% higher carbon monoxide conversion and cobalt-time yield than the same catalyst before the treatment in carbon monoxide with very small modifications of hydrocarbon selectivity.

3.3. In situ XRD characterization of the catalyst structure with simultaneous evaluation of catalytic performance

Before the *in situ* experiments, the catalysts were reduced in hydrogen at 623 K for 2 h. In agreement with previous reports [2,49,56,66–68], the *in situ* XRD data clearly show that reduction of Co_3O_4 proceeds via intermediate formation of CoO. Indeed, CoO was identified from XRD patterns during the pretreatment of cobalt catalysts at 473–523 K in hydrogen. CoO reduction results in formation of cobalt metallic phases. The *in situ* XRD patterns of the $CoPt/Al_2O_3$–N1 and $CoPt/Al_2O_3$–N2 after the reduction at 623 K are shown in Fig. 6. The patterns of the catalysts are constituted by XRD peaks, which can be attributed to cobalt metallic *fcc* and *hcp* phases and γ-Al_2O_3. No distinctive peaks related to CoO and other Co-containing oxide phases were observed. This seems to be consistent with TPR characterization, which is indicative of relatively higher extent of cobalt reduction in both $CoPt/Al_2O_3$–N1 and $CoPt/Al_2O_3$–N2 catalysts in hydrogen at 623 K. Previously conducted XAS experiments [56] with platinum-promoted alumina-supported cobalt catalysts prepared from cobalt nitrate also showed nearly complete cobalt reduction after treatment with hydrogen at 623 K. Somewhat lower extent of cobalt reduction (~90%) was observed by Rønning et al. [49] in rhenium-promoted catalysts after treatment with hydrogen at 673 K. It is known that the effect of rhenium on cobalt reducibility is usually much smaller than that of platinum [4]. XRD patterns suggest that cobalt *fcc* phase is dominant in the reduced catalysts. According to Rietveld analysis, the relative fractions of cobalt *fcc* and *hcp* are, respectively, 80% and 20% in the reduced $CoPt/Al_2O_3$–N1. The XRD patterns are also indicative of lower fraction of cobalt hexagonal phase (or stackings) in $CoPt/Al_2O_3$–N2 catalyst.

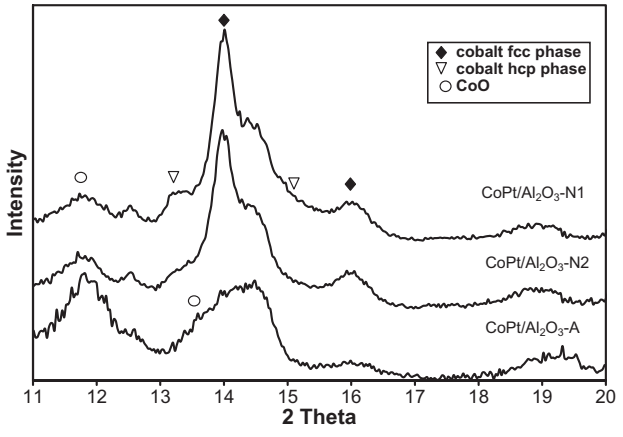

Fig. 6. *In situ* XRD patterns of $CoPt/Al_2O_3$–N1 [50], $CoPt/Al_2O_3$–N2 [50] and $CoPt/Al_2O_3$–A catalysts reduced at 623 K (λ = 0.5 Å).

In contrast to the catalysts prepared from cobalt nitrate, treatment of acetate-derived $CoPt/Al_2O_3$–A catalyst with hydrogen at 623 K results only in partial cobalt reduction (Fig. 6). Indeed, the relevant XRD patterns exhibit broad peaks attributed to residual CoO. This is consistent with TPR data (Fig. 5), which also suggest much more difficult reduction of smaller cobalt oxide particles in $CoPt/Al_2O_3$–A. Even the promotion with platinum does not allow obtaining complete cobalt reduction under these conditions.

Analysis of XRD patterns using full profile matching suggests the presence of cobalt *fcc* metal particles (major phase) of about 6 nm in the reduced $CoPt/Al_2O_3$–N1 and $CoPt/Al_2O_3$–N2 catalysts and cobalt fcc metal particles smaller than 5 nm in $CoPt/Al_2O_3$–A sample. The observed decrease in cobalt particle sizes after reduction compared to the sizes of Co_3O_4 crystallites in the calcined catalysts is consistent with previous studies. Castner et al. [66] showed that the decrease in the volume of cobalt oxide particles after reduction in supported catalysts varies between 30% and 50%. A 20% decrease in crystallite size after reduction from Co_3O_4 to metallic cobalt was earlier uncovered [49] in alumina-supported catalysts using *in situ* XRD.

After the reduction, the catalysts were exposed to syngas at 333 K and the pressure was slowly raised up to 20 bar. Then, the temperature increased to 493 K with a ramp of 1 K/min. No changes of XRD patterns were observed in syngas below 463 K. This is consistent with insignificant rate of FT synthesis at those temperatures. The *in situ* XRD patterns and simultaneously measured catalytic data of the $CoPt/Al_2O_3$–N1 and $CoPt/Al_2O_3$–A measured under syngas flow in the capillary reactor at 493 K and P = 20 bar are shown in Fig. 7. The evolution of XRD profiles with time on stream was different for cobalt catalysts prepared from cobalt nitrate or acetate. A progressive narrowing of metallic cobalt peaks was observed with $CoPt/Al_2O_3$–N1 catalyst (Fig. 7a) during first 3–4 h of FT reaction. Integration of XRD patterns attributed to cobalt metal phases did not show any further cobalt reduction or oxidation in the presence of syngas. This is consistent with

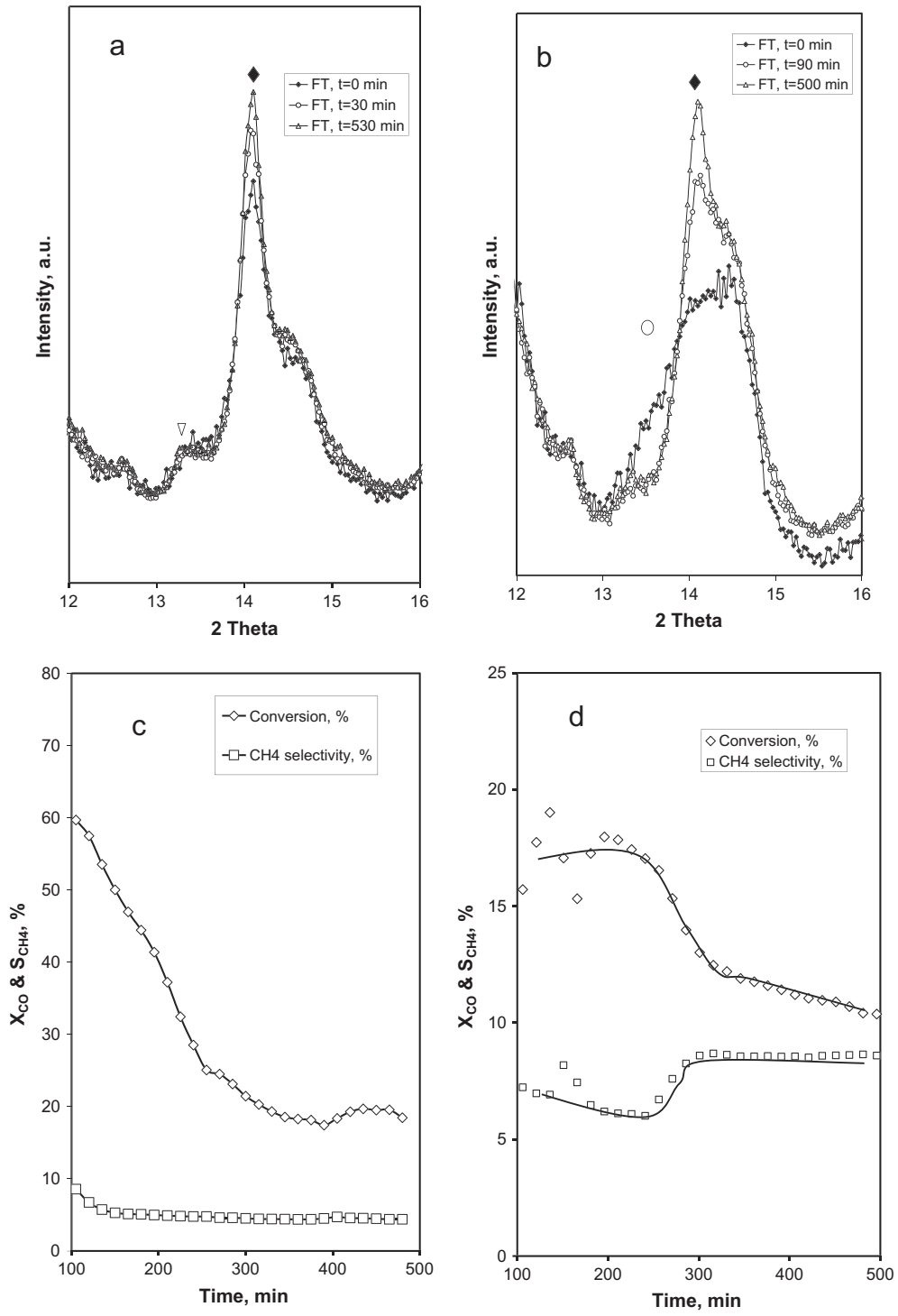

Fig. 7. *In situ* XRD patterns and simultaneously measured carbon monoxide conversion and methane selectivity as functions of time-on-stream for $CoPt/Al_2O_3$–N1 (a and c) and $CoPt/Al_2O_3$–A (b and d) under syngas flow in the capillary cell reactor (T = 493 K, P = 20 bar, H_2/CO = 2 and GHSV = 25,000 ml g^{-1} h^{-1} for $CoPt/Al_2O_3$–N1 and GHSV = 19,600 ml g^{-1} h^{-1} for $CoPt/Al_2O_3$–A).

our conclusion about nearly complete cobalt reduction in this catalyst after treatment in hydrogen at 623 K. It also confirms the data reported by van den Loosdrecht et al. [42] who using *ex situ* characterization have not observed cobalt oxidation in alumina-supported catalysts under industrial conditions of FT synthesis at moderate carbon monoxide conversions. The narrowing of XRD peaks, which are attributed to cobalt metal phases, indicates sintering of cobalt crystallites. The mean diameters of cobalt *fcc* and *hcp* crystallites were calculated from XRD patterns using full profile matching [52] and are displayed in Fig. 8. The sizes of cobalt *fcc* crystallites (cobalt major phase) increase during the first 3–4 h of reaction from 6 to 7 nm, while the size of cobalt *hcp* crystallites (cobalt minor phase) remains relatively stable. In all conducted synchrotron experiments (>7), cobalt sintering was observed in alumina-supported cobalt catalysts under realistic conditions of FT synthesis.

A 20% increase in cobalt metal particle sizes was previously observed by Rønning et al. [49] in rhenium-promoted alumina-sup-

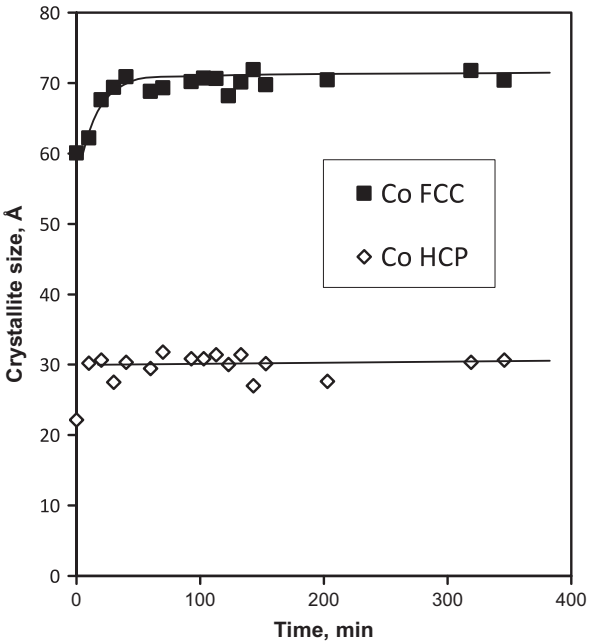

Fig. 8. Evolution of cobalt particle sizes in $CoPt/Al_2O_3$–N1 during FT synthesis (T = 493 K, P = 20 bar, H_2/CO = 2, GHSV = 25,000 ml g^{-1} h^{-1}) calculated using full profile matching (instrument broadening was deduced using standard silicon material).

ported cobalt catalysts using *in situ* XRD experiments, which were conducted at lower syngas pressures (P = 10 bar), higher temperatures (673 K) and space velocities higher than >90,000 ml g^{-1} h^{-1}. In addition, our *in situ* data about cobalt sintering are consistent with very recently published *ex situ* HAADF-TEM analysis of spent $CoPt/Al_2O_3$ catalysts from SASOL demonstration unit [9]. It was observed [9] that cobalt sintering occurs very rapidly during the first days of industrial operation. Interestingly, sintering does not modify the ratio of cobalt *fcc* and cobalt *hcp* metallic phases. In this experiments, sintering of cobalt *fcc* particles was much faster than in our previous report [50], which was probably due to lower space velocity used in the present work (25,000 cm^3 g^{-1} h^{-1} instead of 50,000 cm^3 g^{-1} h^{-1}) and consequently higher carbon monoxide conversion. Apparently, the kinetics of sintering is sensitive to the reactor hydrodynamics, reaction start up and operating conditions. It will be studied in a greater detail in our future work. Simultaneously with cobalt sintering, carbon monoxide conversion dropped from 60% to 20% (Fig. 7c) with methane selectivity being constant at about 6%.

With $CoPt/Al_2O_3$–A catalyst (Fig. 7b), the situation is more complex. In this catalyst, cobalt was not completely reduced after treatment with hydrogen. Under FT reaction conditions, a gradual decrease in the intensity of CoO phase coincided with an increase in the intensity and narrowing of metallic cobalt peaks. This suggests simultaneous reduction and sintering of cobalt particles. These data are consistent with the results of Saib et al. [71] who using XANES observed cobalt gradual reduction in partially reduced cobalt catalysts during FT reaction. Simultaneously with reduction and sintering of cobalt particles in the $CoPt/Al_2O_3$–A catalyst prepared from cobalt acetate, carbon monoxide conversion decreased from 18% to 10% (Fig. 7d), which is indicative of the decrease in the number of cobalt active sites in the catalysts. Note that cobalt sintering can lead either to increase or to decrease in FT catalytic activity, while cobalt reduction should be beneficial for FT activity. In addition, some other deactivation phenomena which are not detectable by *in situ* XRD can occur, e.g. amorphous carbon formation.

Thus, the *in situ* XRD data obtained at moderate carbon monoxide conversions did not show any oxidation of both larger and smaller cobalt metal particles. Note, however, that previous *ex situ* characterization data were sometimes indicative of cobalt oxidation even at very low concentration of water [29–35].

3.4. Carbidization, cobalt fcc and cobalt hcp phases

After longer exposure to syngas (P = 20 bar, H_2/CO = 2, 6–8 h time-on-stream) of alumina-supported cobalt catalysts to syngas, the XRD patterns displayed smaller XRD peaks attributable to Co_2C cobalt carbide [50] in addition to the peaks characteristic of cobalt metal phases and alumina. The amount of cobalt carbide formed in syngas at FT reaction conditions was less than 10% of total cobalt and was more significant in $CoPt/Al_2O_3$–N2 catalyst which was calcined at 773 K than in $CoPt/Al_2O_3$–N1 calcined at 573 K.

In pure carbon monoxide, cobalt metal phases can be readily converted to cobalt carbide almost quantitatively. Fig. 9 shows evolution of *in situ* XRD patterns of $CoPt/Al_2O_3$–N1 catalyst after treatment with carbon monoxide at 493 K and P = 20 bar. In pure CO carbidization proceeds rather quickly; almost all cobalt is converted to cobalt carbide after of 5 h of exposure to carbon monoxide. The average size of cobalt carbide crystallites determined from XRD patterns was about 7.5 nm. After complete carbidization in pure carbon monoxide, the catalyst was exposed to syngas at the same temperature and pressure. The carbidized catalyst has shown zero activity in FT reaction (Table 2). These results are consistent with the catalytic tests conducted in a conventional fixed bed reactor (Table 2), which also do not show any noticeable carbon monoxide conversion on the $CoPt/Al_2O_3$–N1 catalyst which was exposed to carbon monoxide at P = 20 bar at T = 493 K. Previous reports [22,23,26,27] were also indicative of almost compete inactivity of cobalt carbide in FT synthesis. It is important to note that XRD has not shown any structural changes of carbidized cobalt catalyst in the presence of syngas confirming stability of Co_2C under realistic conditions of FT synthesis.

Subsequent treatment of the carbidized cobalt catalyst with hydrogen at 493 K resulted in rapid and selective hydrogenation of cobalt carbide to cobalt metallic phases (Fig. 10). Interestingly, cobalt carbide hydrogenation selectively leads to formation of cobalt hexagonal *hcp* phase, while reduction of cobalt oxide with hydrogen leads selectivity to cobalt cubic *fcc* phase. Rietveld

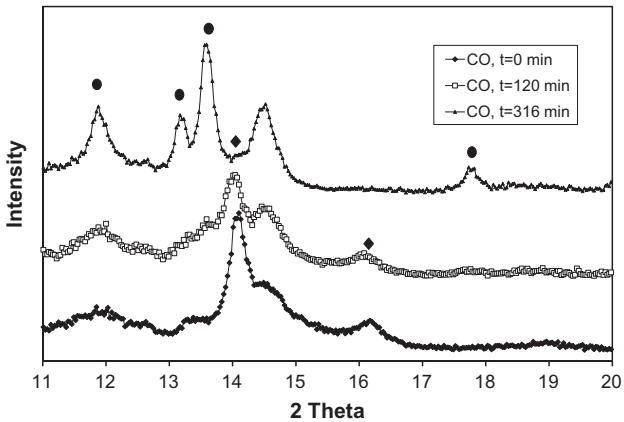

Fig. 9. Evolution of *in situ* XRD patterns of $CoPt/Al_2O_3$–N1 catalyst after treatment with carbon monoxide at 493 K and P = 20 bar (♦ and ● designate cobalt *fcc* metal phase and Co_2C cobalt carbide, respectively).

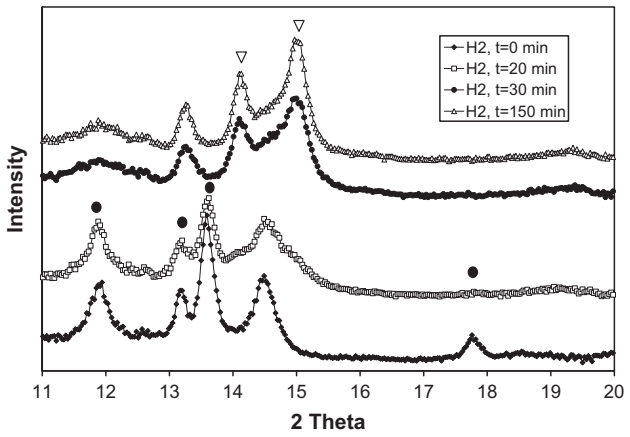

Fig. 10. Evolution of *in situ* XRD patterns of carbidized $CoPt/Al_2O_3$–N1 catalyst after treatment hydrogen at 493 K and $P = 20$ bar (● and ▽ designate Co_2C and Co *hcp* peaks, respectively).

analysis suggests that cobalt metal species are constituted by about 80% of cobalt *fcc* and 20% cobalt *hcp* phases in the $CoPt/Al_2O_3$–N1 catalyst reduced in hydrogen and by about 90% of cobalt *hcp* and 10% cobalt *fcc* phases in the counterpart, which was subjected to carbidization and subsequent hydrogenation. These results are consistent with reports by Anderson and Ducreux [22,26,27]. It is known that reduction of cobalt oxide species supported by alumina results in cubic and hexagonal metal phases. The *fcc* and *hcp* cobalt phases are closed packed structures, which differ only in the stacking sequence of atomic planes in the (1 1 1) direction. The cubic phase is thermodynamically favored at higher temperatures, while the *hcp* phase is more stable at lower temperature. Crystallite size analysis using full profile machining was indicative of the presence of cobalt *hcp* particles of 9 nm. Interestingly, the mean particles size of cobalt *hcp* phase does not evolve during FT reaction, while the catalysts containing higher fraction of cobalt *hcp* phase showed some deactivation in the XRD capillary cell reactor.

The $CoPt/Al_2O_3$–N1 catalyst, which contained mostly cobalt *hcp* phase obtained via carbidization–hydrogenation showed higher activity in FT synthesis than its counterpart containing mostly cobalt *fcc* phase. These results are in agreement with earlier works by Ducreux [26,27]. Note that in previous works [26,27] the catalytic tests were conducted at methanation regime at $P = 3$ bar and $H_2/CO = 9$, which are not representative of realistic FT reaction conditions. The catalytic performance data obtained in the present work in the *in situ* XRD cell operating at $H_2/CO = 2$ and total pressure of 20 bar are in agreement with the results obtained in the steady-state regime with conventional laboratory fixed reactor (Table 2). Indeed, carbidization and hydrogenation of $CoPt/Al_2O_3$–N1 catalysts in the fixed bed reactor led to a 50% increase in carbon monoxide conversion (Table 2).

Note that cobalt *fcc* phase was the major phase in the catalysts reduced in hydrogen, while in the catalysts after carburization–hydrogenation the dominant cobalt phases was cobalt *hcp*. Cobalt mean *fcc* crystallite size in the catalysts after initial sintering was about 7 nm, while in the carburized–hydrogenated catalyst cobalt *hcp* crystallite size was about 9 nm. Assuming spherical shape of cobalt particles containing either cubic or hexagonal phases a higher concentration of cobalt surface sites can be suggested in cobalt catalysts prepared conventional reduction in hydrogen than in the catalyst which was carbidized and then treated with hydrogen. Therefore, FT turnover frequency (reaction rate normalized by the number of active sites) is likely to be higher for cobalt hexagonal phase than for cobalt cubic phase.

3.5. Stability of cobalt metal particles in the presence of water

Analysis of *in situ* XRD patterns did not reveal any cobalt re-oxidation during FT synthesis at moderate carbon monoxide conversions (<30%) in the catalysts containing either smaller or larger cobalt particles. Moreover, cobalt reduction was observed in the partially oxidized catalysts containing smaller cobalt particles under the reaction conditions (Fig. 7b). Indeed, previous thermodynamic calculations and experimental results indicate stability of cobalt particles larger than 4 nm or even 2 nm in syngas under typical conditions of FT synthesis [9,28]. Water is a major product of FT synthesis. Higher carbon monoxide conversion usually results in higher water partial pressure in the reactor. Thus, smaller cobalt metal particles could become less resistant to oxidation in the presence of water at higher carbon monoxide conversion levels. To investigate the stability of cobalt particles at higher carbon monoxide conversion, the *in situ* experiments were conducted with water, which was added to the syngas feed. Previous thermodynamic calculations [28] suggest that at $H_2O/H_2 > 1.5$ in syngas, cobalt metal particles smaller than 5 nm can oxidize to CoO.

Fig. 11 shows *in situ* XRD patterns and catalytic performance data obtained after water addition to FT reaction feed ($H_2O/H_2 = 1.35$) for $CoPt/Al_2O_3$–N1 and $CoPt/Al_2O_3$–A. As expected, no cobalt oxidation detectable by XRD was observed for cobalt catalysts with larger cobalt particles prepared via cobalt nitrate route (Fig. 11a), and very minor cobalt oxidation was observed in the catalysts with smaller cobalt particles prepared from cobalt acetate (Fig. 11b). In the latter case, very small decrease in the intensity of XRD patterns attributed to cobalt metallic phases and small increase in the intensity of CoO XRD peaks could be indicative of some oxidation of cobalt species in the presence of water. Oxidation probably occurs first on the surface cobalt metal particles.

These data are consistent with previous report by van de Loosdrecht et al. [42] who observed relatively higher stability of larger cobalt metal particles in the presence of water. Bezemer et al. [19] also did not see cobalt oxidation in model H_2O/H_2 mixtures in carbon nanofiber-supported catalysts using Mossbauer spectroscopy. Note, however, that XRD analysis is principally sensitive to the phase bulk composition. From the obtained results, it is obvious that cobalt bulk oxidation is not significant during FT synthesis even at higher water concentrations. At the same time, partial oxidation of cobalt surface, which would result in the significant decrease in the number of active sites, cannot be ruled out in the presence of water higher concentrations.

The characterization data are also consistent with the results of catalytic evaluation (Fig. 11c and d). Indeed, addition of water leads to a drop of carbon monoxide conversion and methane selectivity. Previously, lower methane selectivity in the presence of water was observed by Holmen and co-workers [72,73]. Lower carbon monoxide conversion in the presence of water can be attributed, however, to a higher feed space velocity and smaller reactant residence time after water addition. The decrease in carbon monoxide conversion was less pronounced with $CoPt/Al_2O_3$–A catalyst. On this catalyst, an important carbon dioxide production was observed after the addition of water to FT feed.

3.6. Cobalt species in alumina-supported catalysts and their versatility during FT synthesis

The *in situ* XRD data combined with simultaneous evaluation of FT reaction rate and hydrocarbon selectivities have provided important information about the evolution of the structure of calcined-supported cobalt catalysts and their catalytic performance under the realistic conditions of FT synthesis. Fig. 12 illustrates modifications of the structure of alumina-supported cobalt catalysts, which can occur during activation and FT reaction.

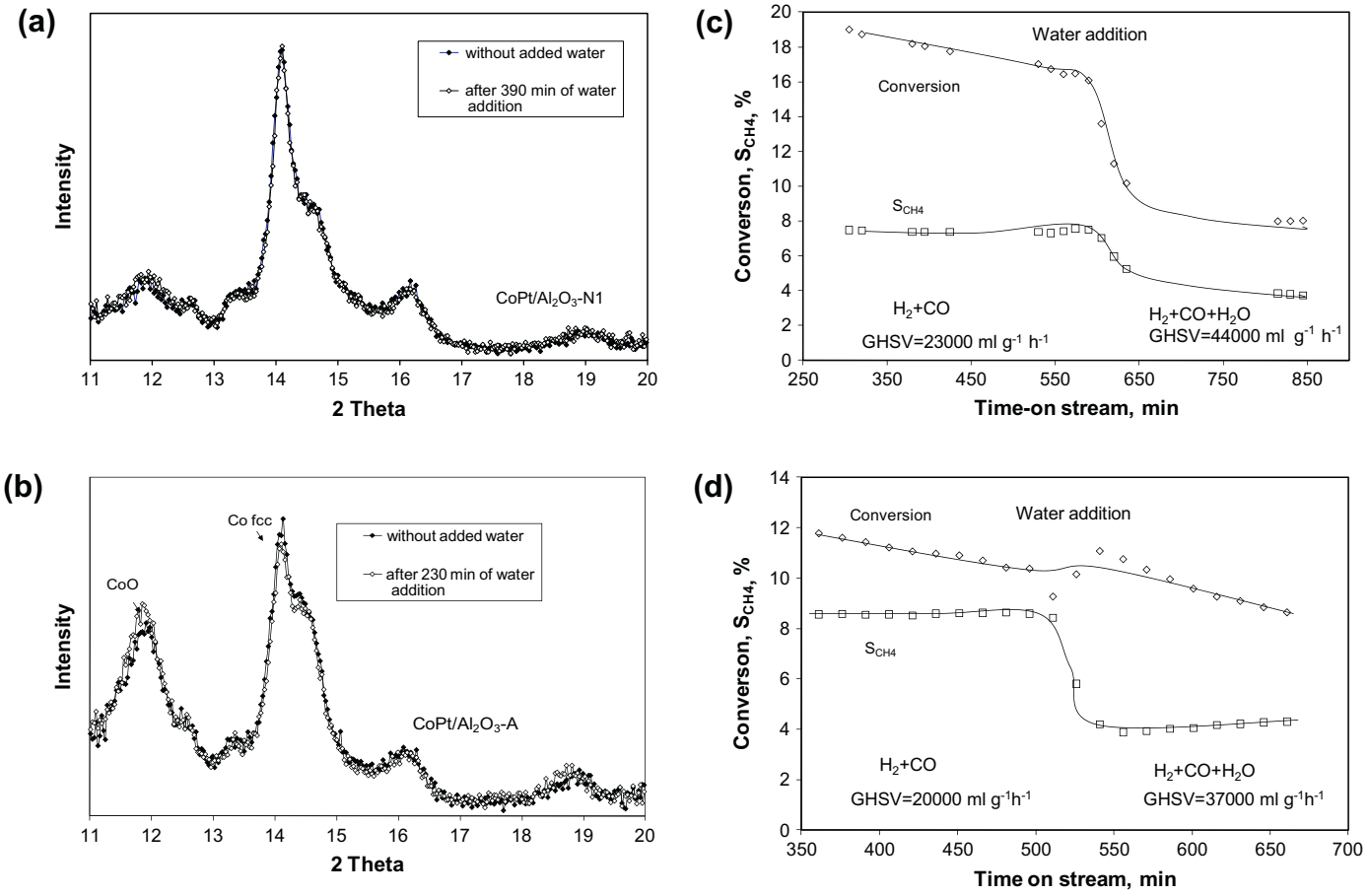

Fig. 11. Evolution of *in situ* XRD patterns and catalytic performance after water addition to FT reaction feed (P = 20 bar, T = 493 K, H_2/CO = 2, H_2O/H_2 = 1.35) for $CoPt/Al_2O_3$–N1 (a and c) and $CoPt/Al_2O_3$–A (b and d).

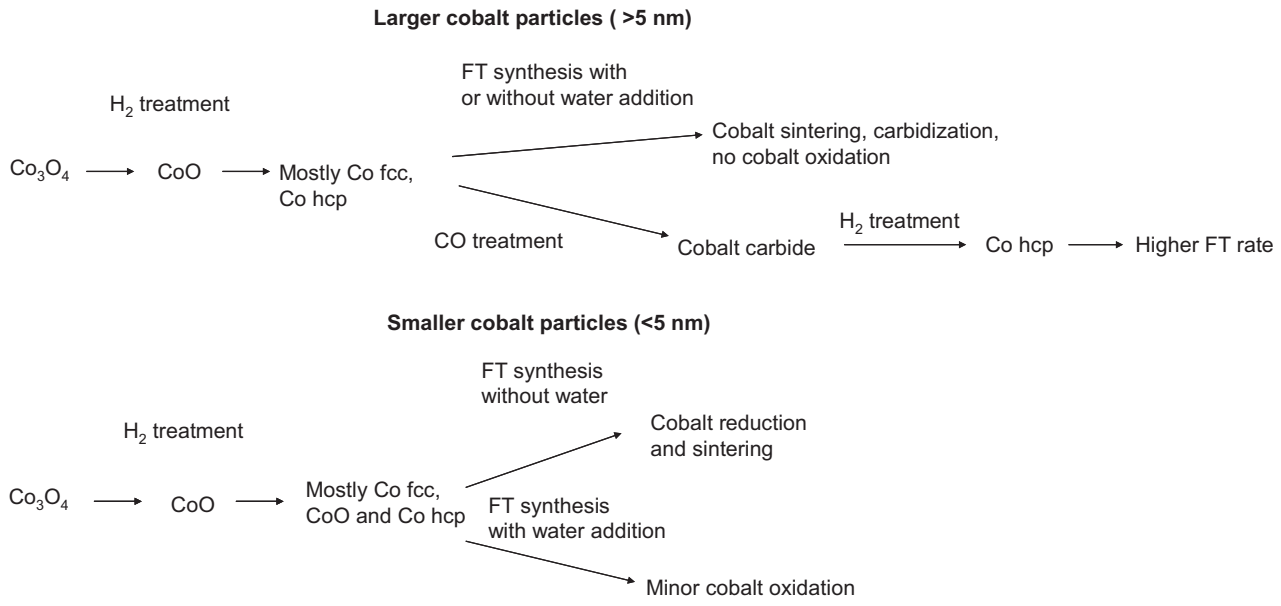

Fig. 12. Modifications of the structure of alumina-supported cobalt catalysts during activation and FT reaction.

Decomposition of cobalt nitrate or acetate and tetramine platinum nitrate in alumina-supported catalysts followed by calcination in air flow results in Co_3O_4 nanoparticles which were identified by XRD and XAS. The sizes of cobalt oxide particles are affected by cobalt precursor. Smaller cobalt oxide particles were detected in the catalysts prepared using cobalt acetate, while

impregnation and decomposition of cobalt nitrate resulted in larger cobalt oxide crystallites (Table 1). XANES data uncovered very low concentrations of cobalt aluminate in all the calcined catalysts promoted with platinum. The catalysts exhibited different reducibility in hydrogen. With cobalt catalysts prepared from cobalt nitrate, catalyst calcination at higher temperatures resulted in more difficult reducibility of cobalt oxide which could be attributed to partial substitution of Co^{3+} in Co_3O_4 spinel lattice with Al^{3+} ions [56]. Impregnation of alumina with cobalt acetate and subsequent calcination lead to smaller cobalt oxide particles and hence to a more difficult reducibility of cobalt species. In agreement with XAS data, TPR showed very low concentrations of cobalt aluminate species reducible at temperatures higher than 873–973 K [74,75].

Treatment of calcined cobalt catalysts in hydrogen at 623 K results in the reduction of cobalt oxide to metallic cobalt. *In situ* XRD data showed that this reduction proceeds via intermediate formation of CoO. Cobalt cubic (*fcc*) phase seems to be dominant in the catalysts reduced in hydrogen at 623 K. The complete cobalt reduction can be attained in the Pt-promoted catalysts prepared using cobalt nitrate ($d_{Co} > 5$ nm), while cobalt is only partially reduced to metallic phase in $CoPt/Al_2O_3$–A, which contains smaller cobalt particles ($d_{Co} < 5$ nm). One of the reasons responsible for more difficult reducibility of smaller cobalt particles to metal phase can be attributed to the thermodynamics [28]. Another reason could be a more difficult stabilization of smaller metal particles relatively to smaller metal oxide clusters on alumina support because of epitaxy constrains. It is expected that an oxide support could more easily accommodate cobalt oxide than cobalt metal particles.

Exposure of the reduced catalysts to syngas with $H_2/CO = 2$ and $P = 20$ bar at 493 K in both conventional laboratory scale fixed bed and *in situ* capillary reactors results in hydrocarbon production. Interestingly, FT reaction rates at steady-state conditions were rather similar in both *in situ* capillary cell and laboratory fixed bed reactor (Table 2). This suggests that the *in situ* XRD cell satisfactorily mimics the kinetics of FT synthesis on the alumina-supported cobalt catalysts in the conventional laboratory scale fixed bed reactor.

The *in situ* XRD experiments exhibited considerable changes in the catalyst structure and catalytic performance during the first 3–5 h of the reaction. Analysis of XRD patterns of the catalysts prepared from cobalt nitrate with higher extent of reduction indicates cobalt sintering, which is accompanied by the decrease in FT reaction rate. It seems that cobalt sintering is one of the principal mechanisms of the initial deactivation of alumina-supported cobalt catalysts under the realistic conditions of FT reaction. No modification of the integral intensity of XRD peaks attributed either to cobalt *fcc* or to *hcp* phase was observed under these conditions in the catalysts prepared from cobalt nitrate which contain larger cobalt particles. This suggests that no cobalt oxidation or reduction occurs under these conditions. Longer exposure of cobalt catalyst to syngas results in appearance of low-intense XRD peaks [50], which can be assigned to cobalt carbide species. The formation of cobalt carbide results in a decrease in the intensity of metallic cobalt *fcc* peaks and thus in the concentration of cobalt metallic phases. It can be suggested that cobalt carbide preferentially forms on the surface of cobalt metal particles and formation of cobalt carbide could contribute to the loss of catalytic activity. Cobalt carbide species can be hydrogenated to metallic cobalt under hydrogen.

Different phenomena were observed with $CoPt/Al_2O_3$–A catalyst, which contains smaller cobalt particles. Because of more difficult reducibility of smaller cobalt oxide particles [64], this catalyst was only partially reduced after treatment in hydrogen at 623 K. Interestingly, no cobalt oxidation was observed with partially reduced cobalt species under the realistic conditions of FT synthesis at carbon monoxide conversion lower than 20%. Exposure of this catalyst to FT reaction medium leads to the reduction of cobalt species. These data suggest that cobalt oxidation (either bulk or surface) cannot be a dominant mechanism of catalyst deactivation at moderate level of carbon monoxide conversion in cobalt catalysts containing either larger or smaller cobalt particles. These results are also consistent with previous data of Rønning et al. [49] who also did not observe in the initial period of the reaction (5 h) any cobalt oxidation in syngas with partially reduced rhenium-promoted Co/Al_2O_3 catalysts. Moreover, exposure of the $CoPt/Al_2O_3$–A catalyst to syngas led to the reduction of residual cobalt oxide species to metallic cobalt (Fig. 7b). Reduction of cobalt oxide species under the realistic conditions of FT synthesis was observed in previous reports [42,43] using *ex situ* characterization. The present *in situ* direct characterization work is consistent with those earlier findings.

Treatment of the catalysts with pure carbon monoxide at 493 K and 20 bar resulted in rapid transformation of metallic cobalt species to cobalt carbide. The mean sizes of cobalt carbide and cobalt metallic crystallites were similar. In agreement with results of Anderson et al. [22], catalytic measurements showed zero activity of supported cobalt carbide in FT reaction. Treatment of cobalt carbide with hydrogen leads to the selective formation of cobalt metallic *hcp* phase. The sizes of cobalt *hcp* crystallites were close to the particle sizes of cobalt carbide. No particle size increase was observed during FT reaction with cobalt catalysts containing higher fraction of cobalt *hcp* phase. Both catalytic tests in the conventional laboratory scale fixed reactor and in the *in situ* XRD units showed higher intrinsic activity of the cobalt sites in the *hcp* phase relative to cobalt *fcc* phase. Ducreux [27] attributed higher activity of cobalt *hcp* phase to easier dissociation of carbon monoxide and enhanced formation of cobalt carbide intermediates. It appears, however, that the reasons of this higher intrinsic activity of cobalt *hcp* phase could be more complex and probably require further investigations, involving analysis of the reactivity of active sites and elementary steps using molecular modeling.

Exposure of cobalt catalysts with larger cobalt particles (>5 nm) to syngas containing higher water concentrations ($H_2O/H_2 = 1.35$) did not result in any noticeable cobalt oxidation. This confirms previously conducted thermodynamic results [9,28] about stability of larger cobalt metal particles in the presence of water even at relatively high concentrations. No immediate and noticeable decrease in FT reaction rate was observed at these conditions. Small decrease in the concentration of cobalt metal phase was observed; however, when cobalt catalysts with smaller metal particles (<5 nm) were exposed to the syngas–water mixture. Thus, though cobalt oxidation is not probably one of the major deactivation mechanisms under the realistic conditions of FT synthesis, it cannot be ruled out for smaller cobalt particles (<5 nm).

The melting point of cobalt is at 1768 K. This gives the Tamman and Hüttig temperatures [5] for cobalt, respectively, at 884 and 530 K. Hüttig temperature is relevant to the mobility of defects, while Tamman temperature is relevant to the mobility of bulk atoms. Alumina-supported cobalt catalysts are stable under hydrogen or inert atmosphere (in the absence of water) at 493 K and even higher temperatures but exhibit a remarkable versatility under the conditions of FT reaction. Thus, the structural changes of cobalt alumina cannot be simply attributed to the temperature effects on atom or particle mobility. It appears that restructuring of cobalt catalyst probably proceeds via interaction of cobalt species with the reacting medium (e.g. carbon monoxide, water, oxygenates, hydrocarbons, etc.) and formation of cobalt mobile intermediate compounds.

The catalyst restructuring observed in this paper using diffraction techniques are principally relevant to crystalline phases. Other catalyst deactivation phenomena, which would involve either formation of amorphous phases, e.g. build-up of amorphous coke/carbon species [76] or mechanisms characteristic for a specific reactor

and reaction conditions (e.g. attrition in slurry bubble column or catalyst poisoning with unclean syngas) were not considered in this work and cannot be ruled out from the present data.

4. Conclusion

The direct characterization using *in situ* XRD combined with simultaneous analysis of the reaction products by on-line gas-chromatography has clearly shown considerable structural versatility of alumina-supported cobalt catalysts promoted with platinum under the realistic conditions of FT reaction. Cobalt sintering and minor carbidization occur at the first hours of FT reaction and result in a decrease in catalytic activity. Partially reduced cobalt catalysts can undergo further reduction under the realistic conditions of FT synthesis. Catalyst exposure to carbon monoxide leads to rapid cobalt carbide formation. Cobalt carbidization followed by hydrogenation selectively led to cobalt *hcp* phase, which seems to be more active than cobalt *fcc* phase in FT reaction. No cobalt oxidation is observed at moderate carbon monoxide conversion. Cobalt oxidation by water is not significant in the cobalt catalysts with larger cobalt particles (>5 nm).

Acknowledgments

The authors are grateful to C. Cucuzzella for TEM measurements and to S. Nikitenko for XAS measurements. The authors would like to thank D. Balloy and P. Recourt for the SEM-EDX analyses. The authors gratefully acknowledge financial support by TOTAL and technical support from SNBL. The ESRF is acknowledged for use of synchrotron radiation.

References

[1] E. Iglesia, S.C. Reyes, R.J. Madon, S.L. Soled, Adv. Catal. 39 (1993) 221.
[2] A.Y. Khodakov, W. Chu, P. Fongarland, Chem. Rev. 107 (2007) 1692.
[3] G.L. Bezemer, J.H. Bitter, H.P.C.E. Kuipers, H. Oosterbeek, J.E. Holewijn, X. Xu, F. Kapteijn, A.J. van Dillen, K.P. de Jong, J. Am. Chem. Soc. 128 (2006) 3956.
[4] F. Diehl, A.Y. Khodakov, Oil Gas Sci. Technol. 64 (2009) 11.
[5] J.A. Moulijn, A.E. van Diepen, F. Kapteijn, Appl. Catal. A 212 (2001) 3.
[6] F. Morales, B.M. Weckhuysen, Catalysis (Roy. Soc. Chem.) 19 (2006) 1.
[7] C.H. Bartholomew, Appl. Catal. A 212 (2001) 17.
[8] N.E. Tsakoumis, M. Rønning, Ø. Borg, E. Rytter, A. Holmen, Catal. Today 154 (2010) 162.
[9] A.M. Saib, D.J. Moodley, I.M. Ciobîcă, M.M. Hauman, B.H. Sigwebela, C.J. Weststrate, J.W. Niemantsverdriet, J. van de Loosdrecht, Catal. Today 154 (2010) 271.
[10] M.E. Dry, Catal. Today 71 (2002) 227.
[11] S. Lögdberg, D. Tristantini, Ø. Borg, L. Ilver, B. Gevert, S. Järås, E.A. Blekkan, A. Holmen, Appl. Catal. B 89 (2009) 167.
[12] M.J. Overett, B. Breedt, E. Du Plessis, W. Erasmus, J. van De Loosdrecht, ACS Division of Petroleum Chemistry, Inc. Preprints 53 (2008) 126.
[13] M. Jacoby, C &E News 86 (2008) 36.
[14] A. Tavasoli, M. Irani, R.M.M. Abbaslou, M. Trepanier, A.K. Dalail, Can. J. Chem. Eng. 86 (2008) 1070.
[15] G. Kiss, C.E. Kliewer, G.J. DeMartin, C.C. Culross, J.E. Baumgartner, J. Catal. 217 (2003) 127.
[16] G. Jacobs, P.M. Patterson, Y.Q. Zhang, T. Das, J.L. Li, B.H. Davis, Appl. Catal. A 233 (2002) 215.
[17] T. Das, G. Jacobs, P.M. Patterson, W.A. Conner, J. Li, B.H. Davis, Fuel 82 (2003) 805.
[18] A. Tavasoli, R.M.M. Abbaslou, A.K. Dalai, Appl. Catal. A 346 (2008) 58.
[19] G.L. Bezemer, T.J. Remans, A.P. van Bavel, A.I. Dugulan, J. Am. Chem. Soc. 132 (2010) 8540.
[20] G. Jacobs, A. Sarkar, Y. Ji, M. Luo, A. Dozier, B.H. Davis, Ind. Eng. Chem. Res. 47 (2008) 672.
[21] F. Fischer, H. Tropsch, Brennstoff. Chem. 7 (1926) 97.
[22] S. Weller, L.J.E. Hofer, R.B. Anderson, J. Am. Chem. Soc. 70 (1948) 799.
[23] J. Xiong, Y. Ding, T. Wang, L. Yan, W. Chen, H. Zhu, Yuan Lu, Catal. Lett. 102 (2005) 265.
[24] R.B. Anderson, W.K. Hall, A. Krieg, B. Seligman, J. Am. Chem. Soc. 71 (1949) 183.
[25] V. Gruver, X. Zhan, J. Engman, H.J. Robota, Prep. Pap. Am. Chem. Soc. Div. Petrol. Chem. 49 (2004) 192.
[26] O. Ducreux, J. Lynch, B. Rebours, M. Roy, P. Chaumette, Stud. Surf. Sci. Catal. 119 (1998) 125.
[27] O. Ducreux, PhD thesis, Université Pierre et Marie Curie, Paris, France, 1999.
[28] E. van Steen, M. Clayes, M.E. Dry, J. van de Loosdrecht, E.L. Vilkoen, J.L. Visagie, J. Phys. Chem. B 109 (2005) 3575.
[29] G. Jacobs, T.K. Das, P.M. Patterson, J. Li, L. Sanchez, B.H. Davis, Appl. Catal. A 247 (2003) 335.
[30] G. Jacobs, P.M. Patterson, T.K. Das, M. Luo, B.H. Davis, Appl. Catal. A 270 (2004) 65.
[31] G. Jacobs, Y. Zhang, T.K. Das, P.M. Patterson, B.H. Davis, Stud. Surf. Sci. Catal. 139 (2001) 415.
[32] G. Jacobs, P.M. Patterson, Y. Zhang, T. Das, J. Li, B.H. Davis, Appl. Catal. A 233 (2002) 215.
[33] T.K. Das, G. Jacobs, P.M. Patterson, W.A. Conner, J. Li, B.H. Davis, Fuel 82 (2003) 805.
[34] J. Li, X. Zhan, Y. Zhang, G. Jacobs, T. Das, B.H. Davis, Appl. Catal. A 228 (2002) 203.
[35] J. Li, G. Jacobs, T. Das, Y. Zhang, B. Davis, Appl. Catal. A 236 (2002) 67.
[36] A.K. Dalai, B.H. Davis, Appl. Catal. A 348 (2008) 1.
[37] M. Bremaud, P. Fongarland, J. Anfray, S. Jallais, D. Schweich, A.Y. Khodakov, Catal. Today 106 (2005) 137.
[38] T.K. Das, W.A. Conner, J. Li, G. Jacobs, M.E. Dry, B.H. Davis, Energy Fuels 19 (2005) 1430.
[39] S. Krishnamoorthy, M. Tu, M.P. Ojeda, D. Pinna, E. Iglesia, J. Catal. 211 (2002) 422.
[40] T.K. Das, X. Zhan, J. Li, G. Jacobs, M.E. Dry, B.H. Davis, Stud. Surf. Sci. Catal. 163 (2007) 289.
[41] F.G. Botes, Ind. Eng. Chem. Res. 48 (2009) 1859.
[42] J. van de Loosdrecht, B. Balzhinimaev, J.-A. Dalmon, J.W. Niemantsverdriet, S.V. Tsybulya, A.M. Saib, P.J. van Berge, J.L. Visagie, Catal. Today 123 (2007) 293.
[43] A.M. Saib, A. Borgna, J. van de Loosdrecht, P.J. van Berge, J.W. Niemantsverdriet, J. Phys. Chem. B 110 (2006) 8657.
[44] M.W.J. Crajé, A.M. van der Kraan, J. van de Loosdrecht, P.J. van Berge, Catal. Today 71 (2002) 369.
[45] J.R.A. Sietsma, J.D. Meeldijk, J.P. den Breejen, M. Versluijs-Helder, A.J. van Dillen, P.E. de Jongh, K.P. de Jong, Angew. Chem. Int. Ed. 46 (2007) 4547.
[46] J. Wilson, C. de Groot, J. Phys. Chem. 99 (1995) 7860.
[47] J.J.C. Geerlings, J.H. Wilson, G.J. Kramer, H.P.C.E. Kuipers, A. Hoek, H.M. Huisman, Appl. Catal. A 186 (1999) 27.
[48] E. Boellaard, A.M. van der Kraan, A.B.P. Sommen, J.H.B.J. Hoebink, G.B. Marin, J.W. Geus, Appl. Catal. A 179 (1999) 175.
[49] M. Rønning, N.E. Tsakoumis, A. Voronov, R.E. Johnsen, P. Norby, W. van Beek, Ø. Borg, E. Rytter, A. Holmen, Catal. Today 155 (2010) 289.
[50] H. Karaca, J. Hong, P. Fongarland, P. Roussel, A. Griboval-Constant, M. Lacroix, K. Hortmann, O.V. Safonova, A.Y. Khodakov, Chem. Commun. 46 (2010) 788.
[51] E.P. Barrett, L.G. Joyner, P.P. Halenda, J. Am. Chem. Soc. 73 (1951) 373.
[52] J. Rodriguez-Carvajal, Physica B 192 (1993) 55.
[53] P. Scherrer, Göttinger Nachrichten, 1918; R. Zsigmondy, Kolloidchemie, third ed., 1920, p. 394.
[54] X.Q. Zhao, S. Veintemillas-Verdaguer, O. Bomati-Miguel, M.P. Morales, H.B. Xu, Phys. Rev. B 71 (2005) 024106.
[55] Y. Wang, C.M. Yang, W. Schmidt, B. Spliethoff, E. Bill, F. Schüth, Adv. Mater. 17 (2005) 53.
[56] W. Chu, P.A. Chernavskii, L. Gengembre, G.A. Pankina, P. Fongarland, A.Y. Khodakov, J. Catal. 252 (2007) 215.
[57] S. Sun, K. Fujimoto, Y. Yoneyama, N. Tsubaki, Fuel 81 (2002) (1583).
[58] N. Tsubaki, S. Sun, K. Fujimoto, J. Catal. 199 (2001) 236.
[59] A. Martínez, C. López, F. Márquez, I. Díaz, J. Catal. 220 (2003) 486.
[60] J. Panpranot, S. Kaewkun, P. Praserthdam, J.G. Goodwin Jr., Catal. Lett. 91 (2003) 95.
[61] J.-S. Girardon, A. Constant-Griboval, L. Gengembre, P.A. Chernavskii, A.Y. Khodakov, Catal. Today 106 (2005) 161.
[62] J.-S. Girardon, A.S. Lermontov, L. Gengembre, P.A. Chernavskii, A. Griboval-Constant, A.Y. Khodakov, J. Catal. 230 (2005) 339.
[63] G.P. Huffmann, N. Shah, J. Zhao, F.E. Huggins, T.E. Hoost, S. Halvorsen, J. Goodwin, J. Catal. 151 (1995) 17.
[64] A.Y. Khodakov, J. Lynch, D. Bazin, B. Rebours, N. Zanier, B. Moisson, P. Chaumette, J. Catal. 168 (1997) 16.
[65] R. Bechara, D. Balloy, J.-Y. Dauphin, J. Grimblot, Chem. Mater. 11 (1999) 1703.
[66] D.G. Castner, P.R. Watson, I.Y. Chan, J. Phys. Chem. 94 (1990) 819.
[67] B. Ernst, A. Bensaddik, L. Hilaire, P. Chaumette, A. Kiennemann, Catal. Today 39 (1998) 329.
[68] A.Y. Khodakov, A. Griboval-Constant, R. Bechara, F. Villain, J. Phys. Chem. B 105 (2001) 9805.
[69] Ø. Borg, E.A. Blekkan, S. Eri, D. Akporiaye, B. Vigerust, E. Rytter, A. Holmen, Top. Catal. 45 (2007) 39.
[70] P.G. Casado, J. Rasines, Solid State Chem. 52 (1984) 187.
[71] A.M. Saib, A. Borgna, J. van de Loosdrecht, P.J. van Berge, J.W. Niemantsverdriet, Appl. Catal. A 312 (2006) 12.
[72] S. Storsæter, Ø. Borg, E.A. Blekkan, B. Tøtdal, A. Holmen, Catal. Today 100 (2005) 343.
[73] S. Storsæter, Ø. Borg, E.A. Blekkan, A. Holmen, J. Catal. 231 (2005) 405.
[74] P. Arnoldy, J.A. Moulijn, J. Catal. 93 (1985) 38.
[75] D.I. Enache, M. Roy-Auberger, R. Revel, Appl. Catal. A 268 (2004) 51.
[76] D.J. Moodley, J. van de Loosdrecht, A.M. Saib, M.J. Overett, A.K. Datye, J.W. Niemantsverdriet, Appl. Catal. A 354 (2009) 102.